Engineering Structures 233 (2021) 111931

Contents lists available at ScienceDirect

Engineering Structures

journal homepage: www.elsevier.com/locate/engstruct

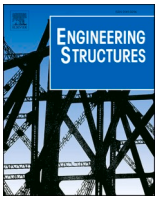

Moving point load approximation from bridge response signals and its application to bridge Weigh-in-Motion

Daniel Cantero

Department of Structural Engineering, Norwegian University of Science & Technology NTNU, Trondheim, Norway

ARTICLE INFO

Keywords:
Bridge
Moving load
Bridge Weigh-in-Motion
Vehicle-bridge interaction

ABSTRACT

This paper presents a revised theoretical interpretation for the analysis of bridge response signals arising during a vehicle passage. The derivation shows that it is possible to approximate the forcing function from bridge responses, by means of a finite difference scheme. This Point Load Approximation (PLA) is also formulated into explicit expressions following classic beam theory. This idea is then generalized to include other load effects and their corresponding time derivatives. These findings are particularly relevant for Bridge Weigh-in-Motion (BWIM) applications. The influence line for a BWIM system with multiple sensors can be explicitly defined using the presented formulation. The theory and applications are validated numerically by means of examples and case studies. These studies include the performance evaluation of a multiple strain sensor BWIM system, as well as, a novel approach to acceleration-based BWIM.

1. Introduction

Road network owners are faced with the challenge of economically managing ever growing infrastructure inventories. To that end, the knowledge of the traffic characteristics has been proven to be a valuable resource for design and management of pavements and bridges [1]. Several countries have used it to even perform bridge condition evaluation [2] and it offers new strategies to prolong asset life [3]. One possibility to obtain this traffic data is by using Weigh-in-Motion (WIM) technology [4]. The most common WIM installation is pavement-based where instrumentation is placed on or near the road surface. This is costly, disruptive to traffic and requires frequent recalibration [1].

Bridge Weight-in-Motion (BWIM) technology instruments a bridge to measure its response during traffic loading to infer axle weights and geometry for every passing vehicle. This alternative offers several advantages compared to the pavement-based solution. The BWIM installation is more durable (sensors not in direct contact with traffic), safer and less disruptive (installation done under the bridge) and more accurate (because of longer duration of the signals) [5]. However, this technology is generally suited only for shorter bridges ($<$20 m).

BWIM was first proposed in 1979 [6] and has been an active field of research ever since. Multiple developments have improved its accuracy and extended its application range, as recent state-of-the-art reviews show [5,7]. In essence, the most common BWIM implementation measures bridge strains during a vehicle passage and compares the signal to the influence line of the measured load effect at the sensor location. Performing a least-squares optimization, results in weight estimates for each of the vehicle's axles. Refer to [8] for extended description of the BWIM technology and its core algorithm.

The influence line is the function that describes the value of a load effect due to a unitary load moving along the bridge. This function is different for each location and load effect and depends on the structural properties and support conditions. There exist several methods to extract it, like the matrix method [9] that calculates it based on the known weights of a calibration truck. Commercially available BWIM systems obtain the influence line as the result of a non-linear optimization procedure [10], based on responses under multiple vehicles of unknown axle weights. However, the problem is far from resolved and has received much attention during recent years. Novel suggestions to find the influence line include: deconvolution in frequency domain [11], regularized least-squares QR factorization [12], adaptive B-splines fitting [13], combination of empirical mode decomposition and Tikhonov regularization [14] and probabilistic method based on the static transmissibility in frequency domain [15].

Influence lines are the cornerstone of BWIM algorithms, and they are arguably the most important feature needed to have accurate weight estimates. It would be advantageous to be able to formulate correct influence lines explicitly. A step towards that goal was suggested in [16–18]. This research shows that it is possible to derive an analytical expression of a generic influence line that is independent of the bridge's boundary conditions, when combining information from various sensors. For a BWIM system based on such an influence line, the input signal is equal to the factored combination of the signals from three strain gauges. This idea, termed Virtual Simply Supported method in [16], was derived theoretically and tested empirically to detect the speed and axle distances of moving vehicles. Subsequently, the same idea was termed

https://doi.org/10.1016/j.engstruct.2021.111931
Received 12 August 2020; Received in revised form 16 December 2020; Accepted 15 January 2021

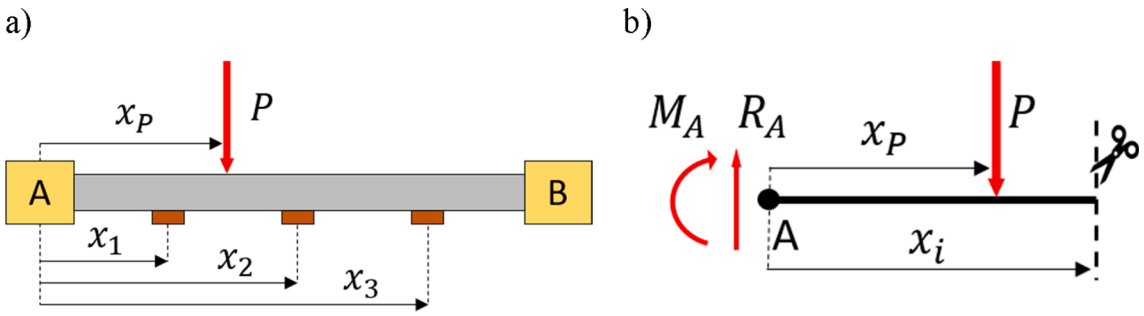

Fig. 1. a) Loaded beam with generic supports and three sensors; b) External and reaction forces to the left of section *i*.

Macro Strain Curvature in [17,18], and was used as the basis for a BWIM system with fibre Bragg grating sensors.

The findings in [16-18] are a leap towards the calculation of robust influence lines for BWIM methods. However, the application range of those findings is limited to strain signals only. Furthermore, the physical interpretation provided is incomplete. A broader and more insightful interpretation is needed. Therefore, the study below further elaborates the underlying theory and extends its applicability to BWIM technology. The results show that the factored combination of signals from several sensors corresponds to a finite difference scheme. This approximate differentiation provides an approximation of the forcing function (moving point load). Moreover, explicit expressions of these approximations can be obtained. This knowledge can be used to develop robust BWIM systems based on multiple sensor readings.

This study aims at presenting a consistent interpretation of previously reported results and its potential for BWIM applications. Section 2 revisits the original derivations in [16-18], to subsequently generalize the results and to integrate them within a more insightful theoretical framework. Section 3 numerically explores the application of the new interpretation for two particular BWIM applications. Finally, the discussion in Section 4 explores the implications of the findings on BWIM technology.

2. Theoretical analysis

In [16-18] the authors derived and explored a useful relationship that combines the measured bending moments from three different sections of a beam solicited by traversing loads. For the case of a unitary moving point load, the combined signal is equivalent to an influence line. Remarkably, it is shown that the shape of this inferred influence line is independent of the boundary conditions. This novel and interesting outcome was termed isolated moment of a point [16] or Macro Strain Curvature (MSC) [17,18] in an attempt to provide a physical interpretation to the result. However, these interpretations are incomplete. This section presents an improved interpretation that generalizes the relationship to other load effects (and not only bending moments).

Furthermore, this section presents a revised derivation with different notation, complemented with additional steps that leads naturally to a better physical interpretation. Whereas in the original derivation [17,18] the strain sensors are considered to have certain length, here we assume that the sensor length is negligible compared to the bridge length. This simplification does not affect the validity or generality of the final result, which could be further extended to account for the length of the sensor. However, the simplification makes the derivation easier to understand and produces smaller expressions.

2.1. Revisited original derivation

A beam with generic supports A and B is loaded by a point load P located at x_P, as depictured in Fig. 1a, for a reference system centred at the left beam support.

Define a section i located at x_i from A and consider the left beam segment for static equilibrium calculation (Fig. 1b). The total moment at that section (M_i) is equal to the sum of moments produced by the load (M_i^P) and by the boundary (M_i^B) as shown in Eq. (1).

$$M_i = M_i^P + M_i^B \tag{1}$$

Following the definitions in Fig. 1b, the moment due to the load P is equal to the piecewise definition (Eq. (2)), depending on what segment of the beam the load is. When the load is on the left segment, then it is simply the product of the force times the distance to the section i. When the load is on the right beam segment, it does not contribute to the equilibrium and has zero value.

$$M_i^P = \begin{Bmatrix} M_{i,1}^P \\ M_{i,2}^P \end{Bmatrix} = \begin{cases} P(x_p - x_i) & if \;\; x_p < x_i \\ 0 & if \;\; x_p \geq x_i \end{cases} \tag{2}$$

The moment from the boundary (M_i^B) is due to the reaction forces at A, namely the vertical force R_A and the support moment M_A, and is defined in Eq. (3).

$$M_i^B = M_A + R_A \cdot x_i \tag{3}$$

Now consider three particular sections along the beam (see Fig. 1a), where we assume to have placed sensors measuring the bending moment. Based on Eq. (3), one can write the theoretically measured moment for each sensor.

$$M_1^B = M_A + R_A \cdot x_1 \tag{4}$$

$$M_2^B = M_A + R_A \cdot x_2 \tag{5}$$

$$M_3^B = M_A + R_A \cdot x_3 \tag{6}$$

These expressions can be combined into a relationship that is independent of the reaction forces. First, subtracting Eq. (5) from Eq. (4) and Eq. (6) from Eq. (5) leads to two expressions that are independent of M_A. These two expressions can then be solved for R_A and compared to each other, resulting in:

$$\frac{M_1^B - M_2^B}{x_1 - x_2} = \frac{M_2^B - M_3^B}{x_2 - x_3} \tag{7}$$

Additional algebraic manipulation of Eq. (7), gives the expression:

$$(x_3 - x_2)M_1^B + (x_1 - x_3)M_2^B + (x_2 - x_1)M_3^B = 0 \tag{8}$$

Next, define the total moment at each sensor using Eq. (1). To take advantage of the relationship in Eq. (8), it is convenient to multiply each by the appropriate factor defined in terms of the sensor coordinates. The resulting expressions are shown here:

$$(x_3 - x_2)M_1 = (x_3 - x_2)M_1^B + (x_3 - x_2)M_1^P \tag{9}$$

$$(x_1 - x_3)M_2 = (x_1 - x_3)M_2^B + (x_1 - x_3)M_2^P \tag{10}$$

$$(x_2 - x_1)M_3 = (x_2 - x_1)M_3^B + (x_2 - x_1)M_3^P \tag{11}$$

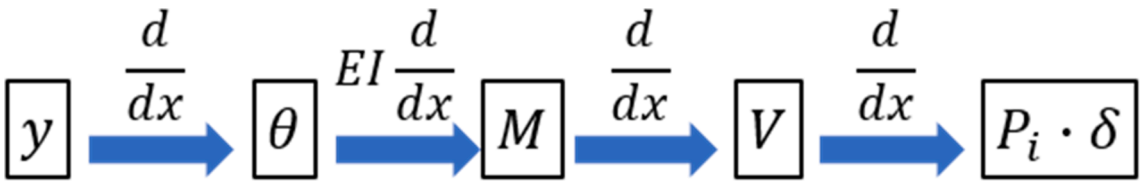

Fig. 2. Schematic relation between load effects and load.

Finally, add together Eq. (9), Eq. (10) and Eq. (11) and use Eq. (2) for each of the considered sensor locations. The final expression presented in Eq. (12) shows that the factored combination of three measured moments is equal to a piecewise function independent of the boundary conditions and defined in terms of the load and the relative location of the sensors to each other. Furthermore, for a traversing unitary load located at x_P, the piecewise function is a triangular shape and could be interpreted as an influence line.

$$(x_3-x_2)M_1+(x_1-x_3)M_2+(x_2-x_1)M_3 = P\begin{cases} 0 & for\ x\in[0,x_1) \\ -(x_3-x_2)(x_P-x_1) & for\ x\in(x_1,x_2) \\ (x_2-x_1)(x_P-x_3) & for\ x\in(x_2,x_3) \\ 0 & for\ x\in(x_3,L] \end{cases} \tag{12}$$

2.2. Extended derivation

Eq. (12) can be further manipulated to arrive to a different and more useful expression. In fact, it is convenient to divide the equation by a factor in such a way that the integral of the right-hand side is equal to P. In other words, to normalize the piecewise function so that the integral of the influence line is equal to the unit. That factor is called here A and is the result of the piecewise integration shown in Eq. (13).

$$\int_0^{x_1} 0dx_P+\int_{x_1}^{x_2} -(x_3-x_2)(x_P-x_1)dx_P+\int_{x_2}^{x_3}(x_2-x_1)(x_P-x_3)dx_P+\int_{x_3}^{L}0dx_P = (x_3-x_2)(x_1-x_3)(x_2-x_1)/2=A \tag{13}$$

Therefore, dividing Eq. (12) by A (Eq. (13)) gives the expression in Eq. (14).

$$\frac{2}{(x_1-x_3)(x_2-x_1)}M_1+\frac{2}{(x_3-x_2)(x_2-x_1)}M_2+\frac{2}{(x_3-x_2)(x_1-x_3)}M_3 = \frac{P}{A}\begin{cases} 0 \\ -(x_3-x_2)(x-x_1) \\ (x_2-x_1)(x-x_3) \\ 0 \end{cases} \tag{14}$$

Upon close examination, one realizes that the factors multiplying the moments on the left-hand side of Eq. (14) correspond to the coefficients of the central finite difference scheme for 2nd order derivative with accuracy 2. This result is for the generic case with irregular spacing between sensors and thus corresponds to the finite difference scheme with a non-uniform grid. For the case of uniformly spaced sensors with a physical separation between them of value h one obtains the more familiar triad of coefficients of the central finite difference scheme, namely $[1,-2,1]/h^2$.

Therefore, one can conclude that in fact the combination of three moments with the factors from the 2nd order finite difference scheme in Eq. (14) is equal to the approximation of its second derivative. As known from classic beam theory, the second derivative of the moment is equal to the load. Consequently, the piecewise function on the right-hand side of the expression is in fact the finite difference approximation of the point load. This insight clarifies why Eq. (14) and the results presented in [16-18] lead to an expression that is independent of the boundary conditions. This is because, indeed, the external load applied to a beam is independent of the support conditions, or even the structure for that matter. The following section aims at extending this revised interpretation to a broader framework to include different load effects.

Table 1
Influence line expressions for a simply supported beam with constant *EI*.

Load effect	Symbol	$I_{LE,i}^{left}$	$I_{LE,i}^{right}$
Shear	V	$\frac{L-x_P}{L}$	$\frac{x_P}{L}$
Bending moment	M	$\frac{L-x_P}{L}x_i$	$-\frac{L-x_i}{L}x_P$
Rotation	θ	$\frac{x_P^2+3x_i^2-6Lx_i+2L^2}{6EIL}x_P$	$\frac{x_P^2+3x_i^2-2Lx_P}{6EIL}(x_P-L)$
Deformation	y	$\frac{x_P^2+x_i^2-2Lx_i}{6EIL}(x_i-L)x_P$	$\frac{x_P^2+x_i^2-2Lx_P}{6EIL}(x_P-L)x_i$

2.3. New interpretation

Euler-Bernoulli beam theory describes the static response of a beam subjected to a point load P located at x_P with the well-known differential equation given in Eq. (15), where δ is the Dirac delta function. This theory relates different load effects on the beam (namely: deformation y, rotation θ, bending moment M and shear force V) to the external load by a series of successive differentiations. Fig. 2 shows a schematic representation of the relations between the involved quantities. This shows that, it is possible to find the forcing function by performing the spatial differentiation (with appropriate order) starting from any load effect.

$$\frac{d^2}{dx^2}\left(EI\frac{d^2y}{dx}\right)=P\cdot\delta(x_P) \tag{15}$$

Strictly speaking, the differential formulation is valid for continuous functions, meaning that the load effects should be known along the length of the beam. However, the relation can be used also to approximate the forcing function with the knowledge of a load effect at only a few spatially distributed discrete locations. The differentiation can be approximated by a finite difference scheme applied to measured load effects at different locations along the beam. In this case the finite difference grid is simply the geometry of the sensor placement. The derivation below obtains the approximation of the forcing function starting from any of the load effects via the finite difference scheme for a generic grid. To that end, the formulation of this idea requires the expressions of the load effects and the appropriate coefficients for the finite difference scheme.

Eq. (16) defines a generic load effect (LE) as a function in terms of a particular sensor location x_i and the location of the point load x_P. This can be written in terms of the influence line ($I_{LE,i}$), which is the load effect at section i of the beam due to a unitary load at x_P. This can be expressed in piecewise form, dividing it in two parts depending on whether the point load is located to the left or to the right of section i.

$$LE(x_i,x_P)=P\cdot I_{LE,i}(x_P)=P\begin{cases} I_{LE,i}^{left}(x_P) & for\ x_P<x_i \\ I_{LE,i}^{right}(x_P) & for\ x_i\le x_P \end{cases} \tag{16}$$

Table 1 shows the influence line expressions for the case of a simply supported beam of length L with constant bending stiffness (EI). These expressions can easily be derived and are readily available in literature but are included here for completeness.

The coefficients of finite difference schemes can be obtained by differentiating the Lagrange polynomials. Refer to [19] for additional information on finite difference schemes and systematic calculation of the coefficients for different differentiation order and accuracy. For example, the coefficients to approximate the 2nd derivative are equal to the 2nd derivatives of the Lagrange polynomials, where the accuracy of the approximation depends on how many nodes are included in the polynomial generation. This method quickly becomes quite cumbersome for hand calculations particularly when considering non-uniform grids and has been completed here with the aid of symbolic calculation software.

Let us denote $\alpha_{X,i}$ as the finite difference coefficient for grid node i to obtain the X order derivative. The coefficients for the central finite difference schemes of order 1–4 with accuracy 2 for uniform and non-uniform grids have been calculated and are listed in the Appendix A.

Now we are equipped with the tools necessary to find an approximation of the forcing function. Any load effect can be written using Eq. (16) and Table 1 and the appropriate differentiation can be approximated by the finite difference scheme with the coefficients listed in Appendix A. Therefore, the forcing function can be approximated using Eq. (17), where n is the number of finite difference grid points, in other words, the number of sensors on the beam.

$$\sum_{i}^{n} \alpha_{X,i} LE(x_i, x_P) = P\delta_{LE}(x_P) \tag{17}$$

The function δ_{LE} approximates the Dirac delta function based on the load effect measured at i locations. The function $\delta_{LE}(x_P)$ is a piecewise function that can be calculated using the expressions of the influence lines and the finite difference coefficients. After algebraic manipulations one obtains the Dirac delta approximations Eq. (18) and Eq. (19) based on the load effects shear and bending moment respectively. The expressions for $\delta_\theta(x_P)$ and $\delta_y(x_P)$ considering non-uniform grids can be computed but are too long to be written down. Appendix B presents their formulation and only for the case of uniformly spaced grids.

$$\delta_V(x_P) = \begin{cases} 0 & x_P \le x_1 \\ -\dfrac{(x_2 - x_3)}{(x_1 - x_2)(x_1 - x_3)} & x_1 < x_P \le x_2 \\ -\dfrac{(x_1 - x_2)}{(x_1 - x_3)(x_2 - x_3)} & x_2 < x_P \le x_3 \\ 0 & x_3 \le x_P \end{cases} \tag{18}$$

$$\delta_M(x_P) = \begin{cases} 0 & x_P \le x_1 \\ -\dfrac{2(x_1 - x_P)}{(x_1 - x_2)(x_1 - x_3)} & x_1 < x_P \le x_2 \\ \dfrac{2(x_3 - x_P)}{(x_1 - x_3)(x_2 - x_3)} & x_2 < x_P \le x_3 \\ 0 & x_3 \le x_P \end{cases} \tag{19}$$

Therefore, this derivation shows that we can approximate the forcing function from multiple load effect measurements on the beam by means of a finite difference approximation of appropriate order. Furthermore, this forcing function can be formulated explicitly (see, Eq. (18) and Eq. (19) and Appendix B) and is independent of the boundary conditions of the beam.

2.4. Static solution examples

In order to clarify the results presented so far, two examples are discussed. The theoretical results are compared to the numerical solution from a finite element model of the beam. Section 3.1 provides additional information about the numerical model used in these examples. Note that these examples deal with the static response of the beam. The contribution of dynamic effects is included in an extended analysis in Section 3.

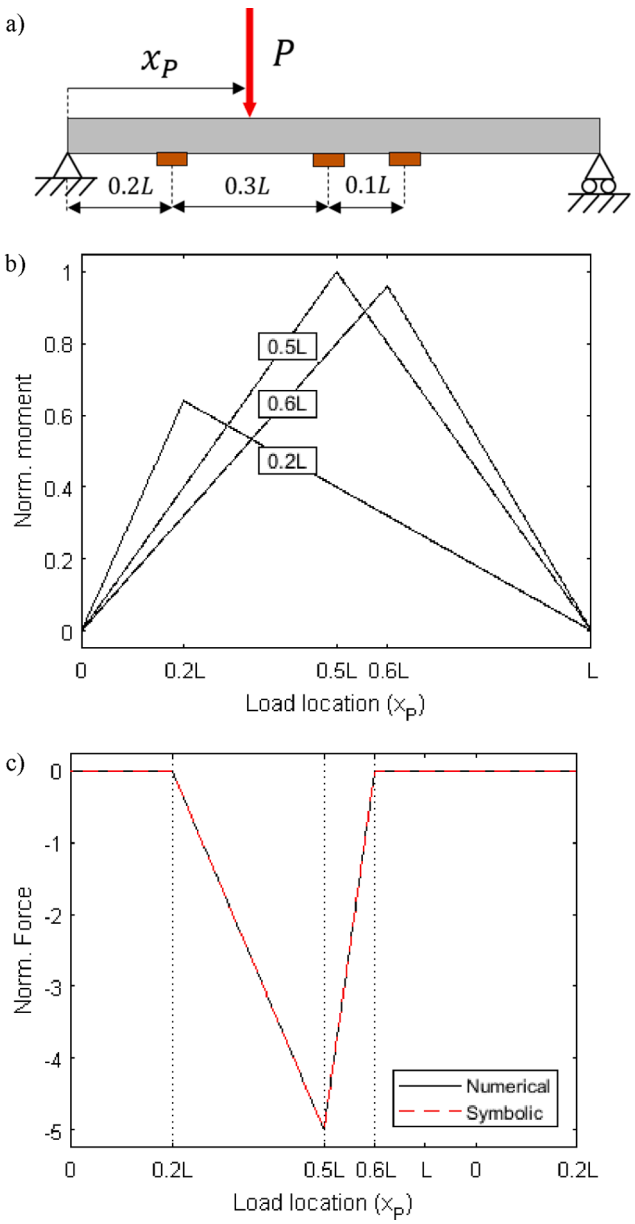

Fig. 3. Example 1; a) Sketch of beam, sensors and load; b) Normalized bending moments for three sensors; c) Forcing function approximation.

The first example is for a simply supported beam traversed by a moving load P. There are three sensors distributed irregularly along the beam (Fig. 3a). These theoretical sensors are capable of measuring the bending moment during the load passage. The measured moments are shown in Fig. 3b, normalized by the maximum mid-span moment. The approximation of the forcing function is calculated numerically and symbolically, rendering the same result (Fig. 3c). The numerical result takes the response of the beam due to the load (Fig. 3b) and applies the 2nd order central finite difference scheme using the coefficients defined in Appendix B. In contrast, the symbolic result in Fig. 3c is calculated using directly Eq. (19).

The second example is for a cantilever beam loaded by a moving constant load P. In this case the sensors measure the vertical deformation and are distributed evenly along the beam (Fig. 4a). The numerical deformation at each sensor in shown in Fig. 4b and normalized by the maximum possible deformation of the beam that is $PL^3/3EI$, which occurs at the free end when the load is placed there. The forcing function

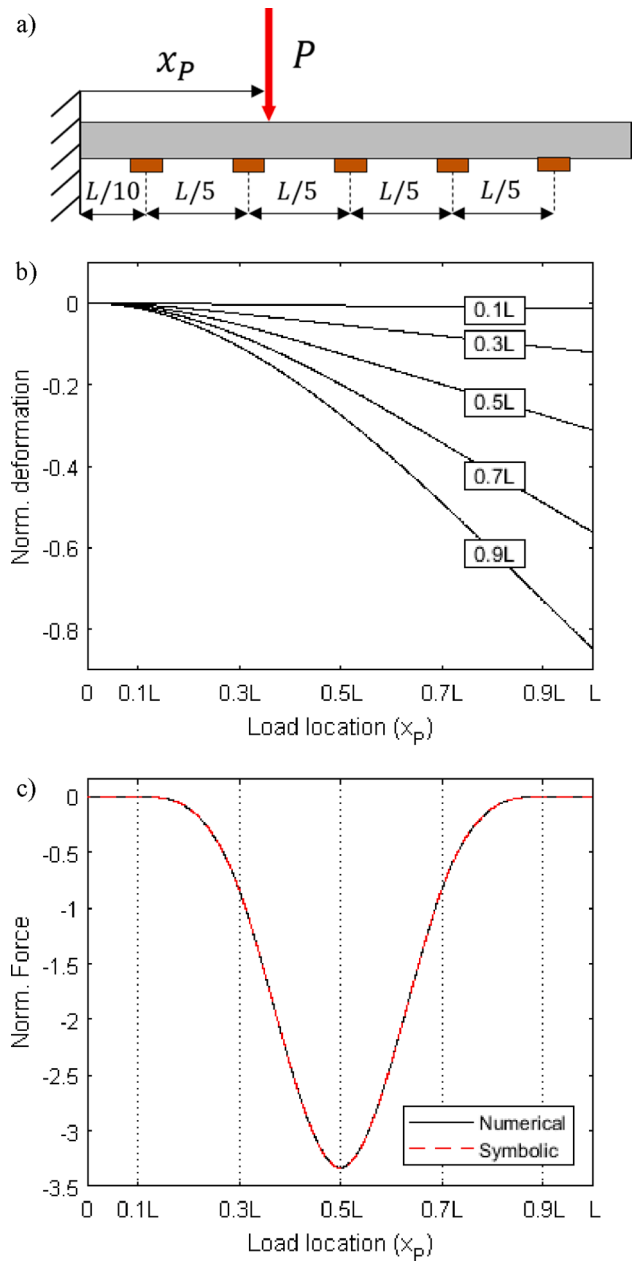

Fig. 4. Example 2; a) Sketch of beam, sensors and load; b) Normalized deformation for five sensors; c) Forcing function approximation.

approximation (Fig. 4c) is obtained numerically by performing the 4th order differentiation using the numerical responses (Fig. 4b) and the corresponding finite difference scheme (Appendix A). This result matches perfectly the symbolic result based on the function δ_y provided in Appendix B.

These examples show that the derived formulation is correct, and therefore that the forcing function can be approximated with explicit formulations. The graphical representations in Figs. 3c and 4c visually highlight some of the properties of the δ_{LE} functions. The load approximations are piecewise functions, where each peace is limited by the sensor locations. The functions are zero-valued outside the grid of points used for the differentiation approximation.

2.5. Generalization

The presented results can be extended to the case of multiple successive traversing loads. Because the formulation of the problem is linear, superposition is applicable. Therefore, Eq. (17) can be extended to include a set of N passing loads (P_j), where each load position is defined by $x_{P,j}$, as seen in Eq. (20). This formulation is applicable to more realistic scenarios where an instrumented bridge is traversed by vehicles with more than one axle.

$$\sum_{i}^{n} \alpha_{X,i} \sum_{j}^{N} P_j I_{LE,i}\left(x_{P,j}\right) = \sum_{j}^{N} P_j \delta_{LE}\left(x_{P,j}\right) \tag{20}$$

In addition, the formulation can be extended in the time domain. We recognize first that the load (vehicle) position changes in time, which is equivalent to make the variable $x_{p,j}$ dependent on time in Eq. (20). Furthermore, it is possible to differentiate the whole equation with respect of time. Eq. (21) shows the generalization of the expression for the m-th order time derivative. The functions I_{LE} and δ_{LE} (given in Eq. (16) and Appendix B) are piecewise polynomial functions that can be expressed in terms of t coordinate. Thus, their m-th order time derivative versions can explicitly be derived, however they have not been reproduced in this document because it was deemed a straightforward operation.

$$\sum_{i}^{n} \alpha_{X,i} \sum_{j}^{N} P_j \frac{d^m}{dt^m}\left(I_{LE,i}\left(x_{P,j}(t)\right)\right) = \sum_{j}^{N} P_j \frac{d^m}{dt^m}\left(\delta_{LE}\left(x_{P,j}(t)\right)\right) \tag{21}$$

Eq. (21) relates any possible load effect (including time-derivatives) to an explicit expression for the approximation of the forcing function (and its time derivatives) via the appropriate finite difference scheme. For example, the equation shows that the 4th spatial derivative of the beam acceleration signals is equal to an explicitly defined function that approximates the (2nd time derivative) forcing function produced by the passing vehicle.

Therefore, the result in Eq. (21) is termed Point Load(s) Approximation (PLA), since it relates approximations of traversing point loads, in explicit form. The left-hand side of Eq. (21) is the factored combination of recorded signals during a vehicle crossing event. The factors are the corresponding finite difference coefficients (Appendix A) defined in terms of the spacing between sensors. Using the correct order for the finite difference scheme results in the approximation of the forcing function, as schematically shown in Fig. 2. The right-hand side of Eq. (21) is also the forcing function approximation but expressed in terms of axle weights and explicit functions. These functions are regularizations of the Dirac delta function for the finite difference grid matching the sensor distribution. These expressions are defined explicitly in Eq. (18), Eq. (19) and Appendix B.

This theoretical result can be used, for instance, to establish a BWIM system using any load effect. The influence line for a PLA-based BWIM system is known explicitly (δ_{LE}) and is independent of the structure. The input signal for the BWIM algorithm is the PLA result, namely the factored combination of several signals via a finite difference scheme. The method requires a minimum number of sensors, which depends on what load effect is measured. There should be at least as many sensors as the number of grid points needed to perform the finite differentiation. The order of the finite difference is the derivative order needed to transform the measured load effect into the forcing function, as known from theory and indicated in Fig. 2.

2.6. Additional comments

This sub-section lists some additional complementary comments to complete the presentation and clarify some aspects of the PLA idea.

- The derivation has been presented for the central finite difference scheme, but other alternatives, such as forward or backward schemes, could also be used.
- The number of grid points used in the finite difference schemes can be increased, and so the number of sensors in an analysis. In that

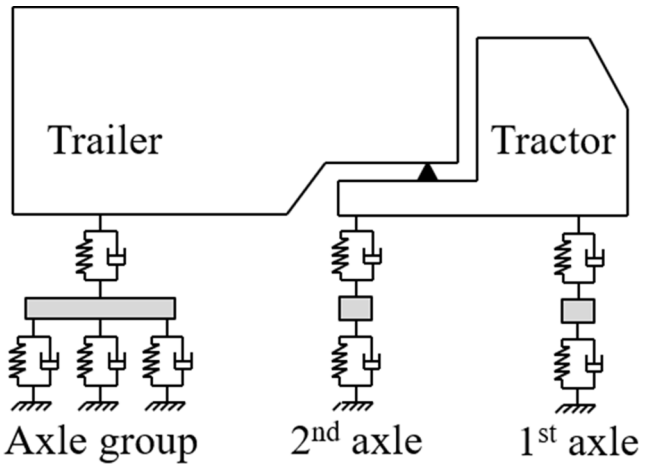

Fig. 5. Sketch of 5-axle truck model.

case, the expressions for the corresponding coefficients become too long to write. However, it is possible to derive them following systematic procedures, as presented in [19], that can be readily implemented and automated.

- Previous derivation was based on the influence line expressions for a simply supported beam (Table 1), for simplicity's sake. Other boundary conditions could have been used resulting in identical δ_{LE} expressions. This is because the load approximation is independent of the structure, as seen in the cantilever beam example (Fig. 4).
- The examples and subsequent analysis in this study assume the knowledge of beam's bending stiffness (EI). However, the actual value of this structural parameter is not strictly necessary to apply the PLA idea since the expressions and results can be left in terms of EI. This facilitates its applicability to real scenarios where this information might be difficult to obtain or is not known exactly.
- The final PLA expression (Eq. (21)) relates only the static components, because the derivation is based on the static description of the loaded beam problem. The derivation does not include damping or inertia effects. However, any load effect measured during a vehicle crossing, features static and dynamic contributions. Some load effects have significant static components (e.g. displacement or strain) while others are dominated by the dynamic contribution (e.g. acceleration). Using signals with deviations from the ideal static response in Eq. (21) introduces errors in the analysis. Therefore, it might be convenient to perform some signal processing on the measurement to (some extent) remove the dynamic component. To that end, one promising possibility is the use of Empirical Mode Decomposition (EMD) as reported in [14,20]

3. Numerical investigations

The presented PLA idea can have potential implications on different applications, ranging from traffic weight estimation to Structural Health Monitoring (SHM). This section explores numerically only two particular applications for BWIM technology, namely, using multiple strain readings and acceleration-based BWIM. However, let us introduce first the model and methods used for the numerical investigation.

3.1. Modelling and analysis

The aim of the numerical model is to simulate heavy trucks passing over a bridge considering realistic conditions and properties for the model. No specific situation is precisely modelled, but rather the model represents a generic vehicle and bridge. The analysis is complemented with Monte Carlo simulations to deal with the inherent uncertainties and variabilities of the problem. Therefore, the model consists of a vehicle moving over a road profile and bridge. The calculated bridge load effects are the inputs for a BWIM system.

The vehicle represents a 5-axle truck, made of rigid bodies (tractor, trailer and axles) connected to the road by suspension and tyre systems, which are modelled as spring and dashpot configurations (See Fig. 5). More details about the development of such numerical models can be found in [21]. The geometry and mechanical properties are based on common values of such 5-axle trucks on European roads and are taken from [22]. This reference also provides the parameters for probabilistic distributions (mean, standard deviation, maximum and minimum values) that are the basis for the generation of random property samples of the vehicle properties for the Monte Carlo analysis. Road profiles are randomly generated following corresponding international standard [23] that provides power spectral density definitions for well-maintained highway roads, which are categorized as Class 'A'. A Finite Element Model (FEM), which has been previously described in [22], is made of 100 beam elements and simulates the bridge. The particular bridge properties values are: 25 m span (L), 18358 kg/m mass per unit length, $4.87 \cdot 10^{10}$N m^2 bending stiffness (EI) and 3% damping, deemed to represent typical properties of a beam and slab construction. The fundamental frequency of the bridge model is 4.09 Hz (f_B) and is in agreement with reported average frequency values of exiting bridges [24].

The main outputs of the dynamic vehicle-bridge simulation are the bridge responses, which are the signals used for the subsequent BWIM analysis. This analysis requires the knowledge of two things, namely the signal of the particular crossing event and the influence line. For the standard BWIM system, the signal is the mid-span strain response and the influence line is the strain at that location due to a unitary load. Alternatively, and based on the theoretical results presented in previous section, one can establish a BWIM system based on multiple signals

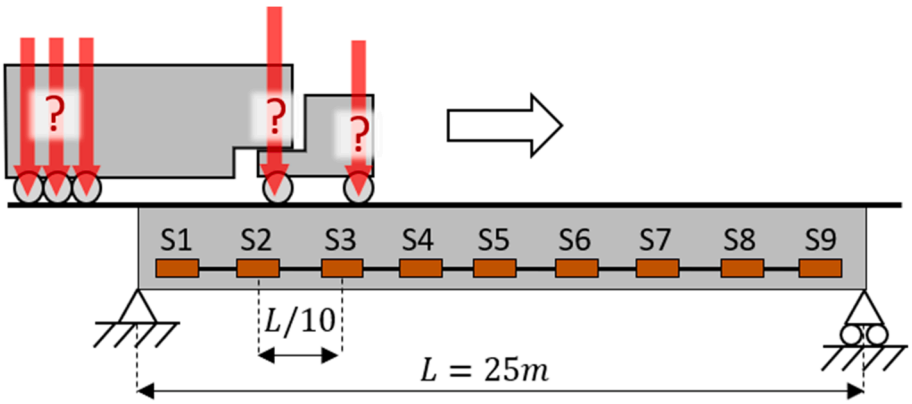

Fig. 6. 5-axle truck crossing a bridge with array of evenly spaced strain gauges.

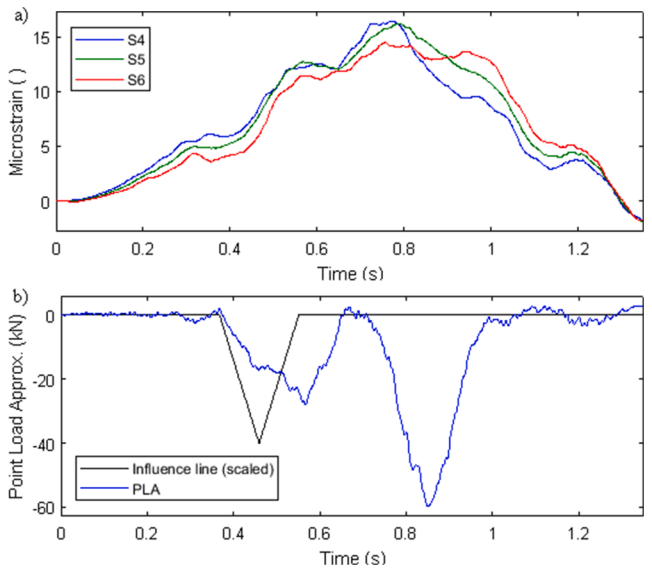

Fig. 7. Results for a 5-axle truck passage; a) Strain signals; b) Point load approximation signal compared to the corresponding influence line.

along the beam. In this case the signal is the PLA (the factored combination of several signals) and the influence line is the corresponding δ_{LE} function according to the measured load effect. It is important to note that the core calculations in both alternatives are the same, i.e., a least-squares optimization that provides individual axle weight estimates. The difference between both alternatives are the input signal and the influence line.

Furthermore, BWIM systems have difficulties estimating individual weights for closely spaced axles, particularly on longer bridges. This problem is avoided considering groups of equally loaded axles, which reduces the number of unknowns and improves the results accuracy. This is a standard procedure currently implemented in modern BWIM systems [25] and relies on the fact that suspension systems evenly distribute the load among the axles within a group. The numerical simulations here consider this axle grouping strategy to calculate the three axle weights of the trailer of the 5-axle truck (Fig. 5). Additionally, the numerical analysis assumes known vehicle entry and exit times as well as the vehicle's axle distance configuration. This information is usually obtained in existing BWIM systems by pre-processing the signals [5].

3.2. BWIM using multiple strain readings

The use of arrays of strain sensors for BWIM systems has been previously explored. Particularly, in [17,18] the authors investigate numerically and experimentally the use of fibre Bragg grating sensors to establish a BWIM system. This optical fibre sensor technology, when installed along the beam, provides multiple closely spaced strain readings. This section revisits the same idea but under the light of the new PLA interpretation.

The simply supported bridge, shown in Fig. 6, is instrumented with 9 evenly distributed strain gauges and traversed by a 5-axle truck with unknown axle weights. The strain signals from each sensor can be transformed to bending moments simply factoring the signals by the bridge's bending stiffness (EI). The 2nd spatial differentiation of the moments gives an approximation of the multiple point loads from the

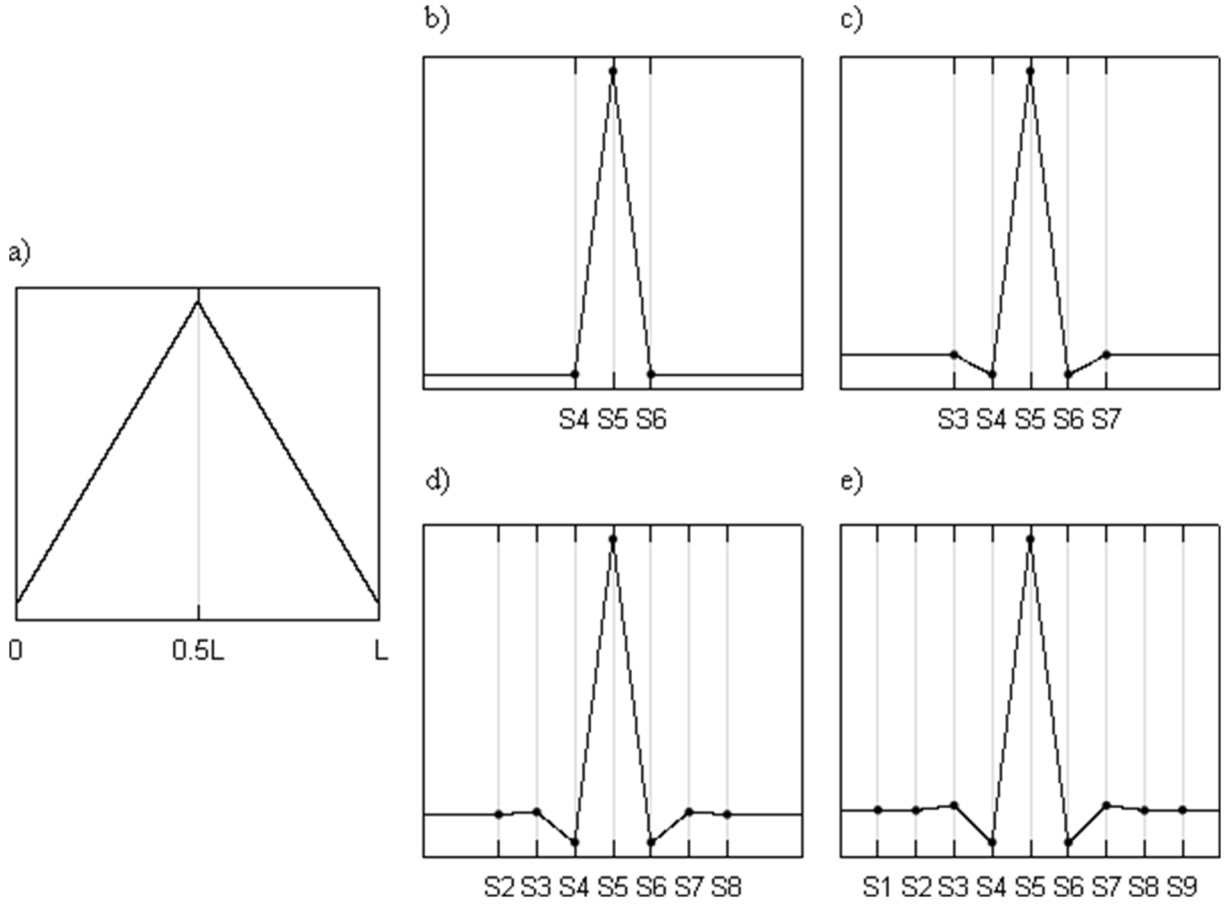

Fig. 8. Examples of influence lines for strain sensors considering. a) 1 sensor; b) 3 sensors; c) 5 sensors; d) 7 sensors; e) 9 sensors.

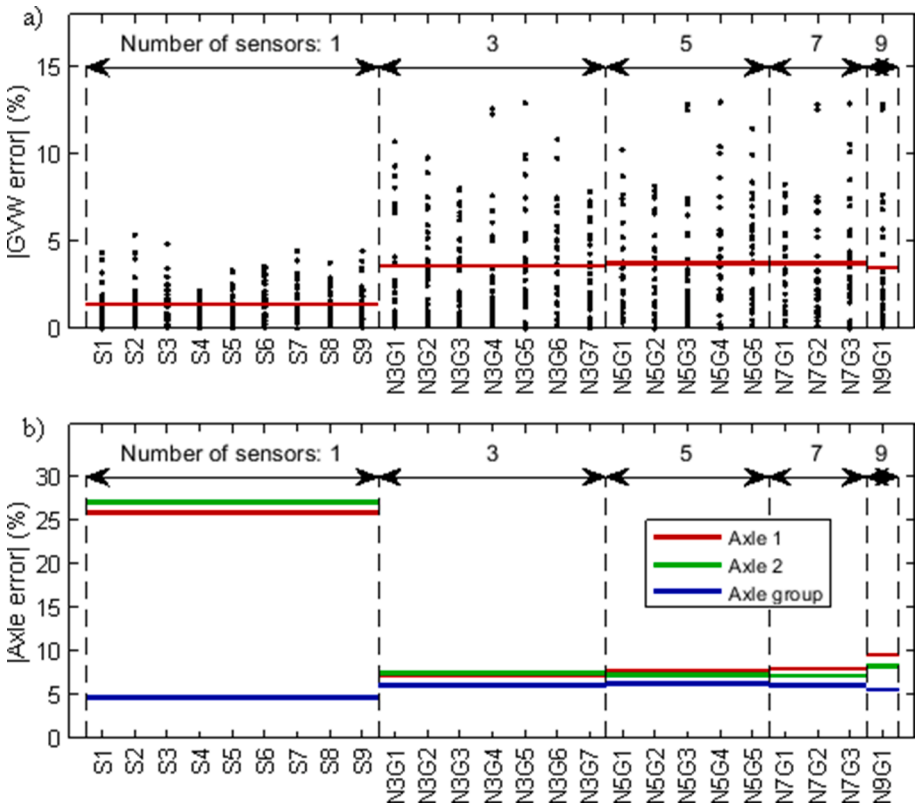

Fig. 9. Strain-based BWIM results for Monte Carlo analysis with 30 events; a) GVW estimation error; b) Axle weights estimation errors.

vehicle.

Fig. 7a shows the strain signals for the sensors near the mid-span (S4, S5 and S6) for one vehicle crossing with a random instance of properties and road profile. The 2nd spatial derivative can be approximated via the central difference scheme using the coefficients in Appendix B. Fig. 7b displays the resulting signal (PLA) compared to the shape of δ_M (see Eq. (19)) for the specific span L and sensor locations. The signal and influence line in Fig. 7b are used to perform BWIM calculations, obtaining a GVW error of −6.1% and errors in tractor axles and trailer axle group estimates of −9.6%, 2.2% and 0.6% respectively.

The standard BWIM uses one single sensor, which for the theoretical case of a simply supported beam with the sensor at mid-span (S5) has a triangular influence line, as shown in Fig. 8a. The new PLA interpretation proposes the generation of influence lines using the signals from multiple sensors, as demonstrated in Fig. 7b using 3 sensors. But in fact, it is possible to combine more signals to obtain PLA influence lines by increasing the number of grid points in the finite difference approximation. For comparison purposes, Fig. 8 shows influence line examples when considering grids with 3, 5, 7 and 9 points. There exist multiple options for grouping the sensors. However, in this study the grouping options have been limited only to groups composed of consecutive sensors and using the notation: N+(number)+G+(group number). For example, N5G2 denotes the group of 5 consecutive sensors starting from S2. The PLA influence lines based on multiple sensors are narrower than the one associated to a single sensor. In theory, BWIM systems using such sharp influence lines should provide good results and improved accuracies on the weight estimates, particularly for closely spaced axles.

Both BWIM alternatives are put to a test by comparing their performances for a sample of randomly generated vehicle and road situations. The first alternative is the classic strain-based BWIM using one single strain gauge. In this example it is possible to define 9 different single sensor BWIM systems, one for each sensor '*S*' shown in Fig. 6. Each installation requires the knowledge of the local influence line and the event's signal, resulting in 9 instances of axle weights estimates of the passing vehicle. Alternatively, for the PLA-based BWIM (with multiple sensors), there are several possibilities depending on the number and location of sensors considered. Now the PLA influence lines for these sensor groups are derived explicitly as exemplified in Fig. 8 and the signals are the factored combination of the recorded strain histories using the relevant finite difference coefficients or PLA.

A Monte Carlo analysis with 30 vehicle crossing events has been simulated, where vehicle speed, payloads and suspension properties, as well as, road profiles have been randomly sampled to represent the variability in the results found in real measurements. Fig. 9a shows the prediction errors in GVW in absolute value for both BWIM alternatives and used sensor combinations. The figure displays the error for each individual event, as well as the average of the 30 runs. It is evident that single sensor BWIM provides more accurate GVW estimates than solutions that have used 3 or more sensors. The reduced accuracy in the PLA-based BWIM estimates is because of the accumulation of signal disturbances. The combination of 3 or more signals that include disturbances due to dynamic effects results in more corrupted signals. This can be observed in Fig. 7. Whereas the individual strain signals are relatively smooth, the PLA signal has noise-like features arising from the factored signal combination. Any deviation from the ideal static signal affects the accuracy of BWIM calculations. The accumulation of signal disturbances on PLA-based BWIM solutions results in larger errors in GVW estimates.

It is well known that standard BWIM generally provides very good estimates for GVW. But ultimately the goal of BWIM systems is to be able to estimate individual axle weights. Then the solutions are more prone to error. In fact, the accuracy of single axle weight estimates is poorer in BWIM systems. This is reflected in the error tolerances of WIM system certification criteria [4], which generally demand higher accuracies for GVW estimates compared to axle groups and single axle estimates.

The same 30 events from the Monte Carlo simulation are investigated to assess individual axle weight estimates. Because of the axle grouping strategy, there are only 3 unknown axle weights for the 5-axle truck, namely those of the first axle, second axle and the trailer's axle group.

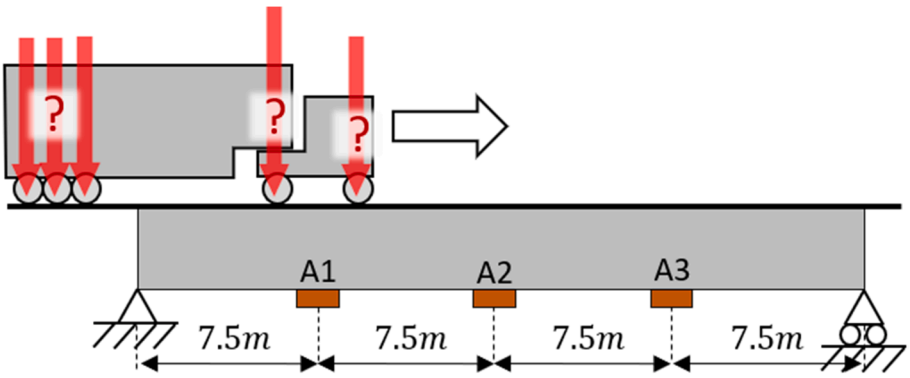

Fig. 10. 5-axle truck crossing a bridge with evenly spaced accelerometers.

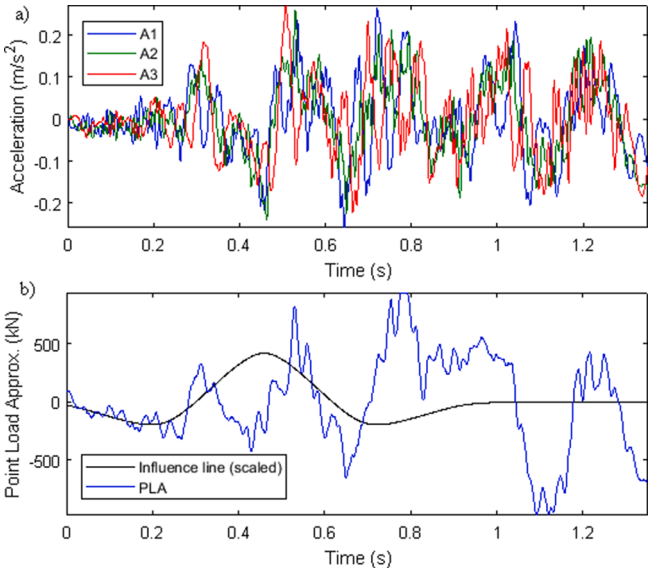

Fig. 11. Results for a 5-axle truck passage; a) Acceleration signals; b) Point load approximation signal compared to the corresponding influence line.

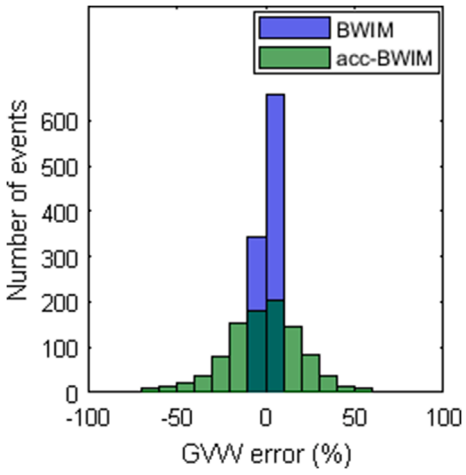

Fig. 12. Histogram of GVW error.

The average weight estimate error for each of these axles (groups) is shown in separate lines in Fig. 9b. The single sensor BWIM provides poor axle weight estimates for the tractor's single axles. The accuracy for the axle group is significantly better, indicating the effectiveness of the axle grouping strategy. On the other hand, PLA-based BWIM systems estimate all axle weights with similar accuracy levels. This alternative drastically improves the accuracy of the individual axle estimates. This improvement can probably be attributed to the use of narrower influence lines and PLA signals, which to some extend transforms the single event into two separate ones. Take the example in Fig. 7b. The PLA signal shows distinct valleys between the times 0.4 s, 0.7 s and 1 s, which could be interpreted as separate events for the tractor and trailer. Arguably, the combination of signals into a single PLA separates their contributions, thus reducing the negative effects from one to the other during the estimation process. However, note that this is only a qualitative explanation. The calculations of both BWIM alternatives consider the whole event as single one and only input signals and influence lines differ. Furthermore, the results in Fig. 9b also seem to indicate that it is not necessarily beneficial to increase the number of sensors in a sensor group.

3.3. Acceleration-based BWIM

In recent years the use of accelerometers for BWIM has been suggested, where ease of sensor installation stands out as the biggest advantage. One possibility is to have a displacement-based BWIM systems where the acceleration signals are double integrated [26], showing decent accuracy on extended monitoring periods [27]. Alternatively, [28] suggests an approach to use an acceleration signal directly on the BWIM algorithm, reporting poor accuracies due to persistent GVW underestimations, but statistically robust to detect an eventual damage on the structure. The numerical study in this subsection explores the use of multiple acceleration signals to obtain an approximation of the loading (PLA) and use that as the basis for the BWIM algorithm.

Fig. 10 shows a schematic description of the numerical example under study, a simply supported beam instrumented with 3 accelerometers traversed by a 5-axle truck with unknown axle weights. The proposed method requires the transformation of the acceleration signals into the (2nd time derivative) loading function, which can be approximated by the 4th order finite difference derivative, as expressed in Eq. (21). The minimum grid size for this approximation is 5 points, while the example assumes the existence of only 3 sensors. This can be resolved by taking advantage of the known behaviour at the supports. One can assume the existence of 2 virtual accelerometers that output constant zero signals. Therefore, 3 real accelerometers and 2 virtual ones provide sufficient information to perform the 4th order differentiation.

Fig. 11a presents the acceleration time histories from the 3 accelerometers for a randomly generated vehicle crossing event. The PLA signal can be calculated considering the additional zero signals from the virtual sensors at the supports and is shown in Fig. 11b. The corresponding necessary PLA influence line ($\ddot{\delta}_y$) is the approximation of 2nd time derivative of the Dirac delta function, which can be derived from the equations in Appendix B, and is also shown in Fig. 11b. Because the acceleration signals are dominated by the dynamic contribution, it is

Table 2
Mean (μ) and standard deviation (σ) of weight estimates error (%) from Monte Carlo simulation with 1000 events.

	BWIM		acc-BWIM	
	μ	σ	μ	σ
GVW	0.46	1.19	−1.5	23.81
Axle 1	−32.18	33.94	−24.58	53.53
Axle 2	25.44	36.85	11.25	33.05
Axle group	0.68	5.59	0.37	23.54

advantageous to apply some form of signal processing to remove most of its effects. In this example, a low-pass filter with a cut-off frequency of 3.27 Hz (=0.8 f_B) is applied to the PLA signal and PLA influence line shown in Fig. 11b. Signal and influence line are used to perform the BWIM calculations, obtaining a GVW error of −2.6% and errors in tractor axles and trailer axle group estimates of −25.3%, 4.0% and 0.8% respectively.

One single example is not representative to assess the performance of the method. Therefore, a Monte Carlo simulation with 1000 randomly sampled vehicle crossing events is used to compare weight estimates from alternative solutions. The reference case corresponds to the standard single mid-span strain sensor BWIM method, which is compared to the acceleration-based BWIM with 3+2 (real + virtual) sensors.

Fig. 12 compares the errors in GVW estimation for both alternatives. The standard strain-based BWIM clearly outperforms the acceleration-based alternative because the distribution of errors is more densely distributed around the zero mark. However, it is interesting to note that even though the deviation in results is larger for the acceleration-based BWIM, the mean value of both is similar and near zero. Furthermore, Table 2 compares the single axles and axle group estimation errors in terms of mean and standard deviation of the results. Both methods perform poorly in terms of average error result, whereas the dispersion is generally greater for the acceleration-based BWIM.

This example has shown that the acceleration-based BWIM does not provide precise results, but they can be useful. In general, variability in weight estimation is larger but produces reasonably good average result, similar as those from the standard BWIM. Additionally, the idea of virtual sensors has been exploited to allow for the required approximate differentiation via a finite difference scheme.

4. Discussion

The PLA idea offers a more insightful framework to utilize the signals from vehicle-bridge crossing events. The potential applications of this interpretation must be further explored. This study has focused on the implications on BWIM technology. However, this exploratory numerical investigation cannot provide a general recommendation on the suitability of the PLA-based BWIM idea. Additional studies are required for different vehicle configurations, bridge properties and sensor configurations, among other defining characteristics of this problem.

Nevertheless, the theoretical framework shows several important features for BWIM technology. Arguably the most important one, is that it is possible to define the exact shape and magnitude of the PLA influence line with an explicit analytical formulation. This shape is made of piecewise polynomials, where each segment is bounded by sensor locations. On the other hand, the influence line in a standard BWIM installation is not defined analytically. The shape of the influence line can be extracted and approximated also as a piecewise function, but the magnitude must be obtained during the calibration process. Furthermore, this influence line might change with temperature or alterations of the support conditions [10]. The PLA influence line overcomes these issues, because it encapsulates the bridge response into an approximation of the traversing load, which is independent of the structure and support conditions. Therefore, a BWIM based on this PLA influence line is advantageous under real operational conditions.

Furthermore, the framework naturally extends the formulation to other load effects. This facilitates the definition of BWIM systems based on alternative sensor solutions. In addition, the PLA idea could be used to implement BWIM systems on longer bridges as opposed to conventional BWIM installations that are only suited for short-span bridges. In a PLA-based solution, the length of the influence line is defined by the distance between the outer sensors. Thus, a BWIM installation could be devised on a long-span bridge by placing sensors that define a shorter influence line. PLA-based BWIM systems using multiple strain signals have already been explored and validated empirically in [16-18]. These studies were based on narrower interpretations of the problem but corroborate the theoretical findings presented above.

A PLA-based BWIM system requires the installation of several sensors along the bridge. This is common practice in some modern installations, which have mid-span sensors and several supplementary strain gauges. These additional signals are currently used for velocity estimation and axle detection. Therefore, the PLA idea could readily be implemented in such installations, requiring only modifications in the analysis of the measured responses. Furthermore, the results in this study show that using PLA-based BWIM can increase the accuracy of individual axle weight estimates, whereas single sensor systems provide better GVW predictions (due to the accumulation of disturbances when combining multiple signals). To take advantage of the strengths of both methods it would be feasible to combine both approaches utilizing the method that provides better accuracy for each estimate respectively.

The practical implementation on a real bridge of a PLA-based BWIM system faces many of the same difficulties as the standard BWIM system. These include, for instance, the influence of the transverse vehicle position and signal corruption by noise. Therefore, the same strategies as for standard BWIM installations can be utilized on PLA-based alternatives. To address the transverse vehicle position issue, BWIM systems combine the signals from several sensors placed along the same cross section. On the other hand, the effect of noise can be reduced by appropriate signal processing, such as low-pass filtering [16].

5. Conclusion

This study has presented the Point Load Approximation (PLA) idea for vehicle-bridge crossing events. Starting from classical beam theory, the derivation has shown that the forcing function can be approximated from multiple measurements on the beam by means of a finite difference approximation of appropriate order. At the same time, this forcing function can also be formulated explicitly. The theoretical finding was integrated into a generalized formulation that extended it to other load effects and corresponding time derivatives. This interpretation offers a broader and more insightful theoretical framework, which integrates results previously reported in other publications.

The PLA idea has then been applied to Bridge Weigh-in-Motion (BWIM) technology and enabled the definition of PLA-based BWIM systems. In these systems, the influence line is defined explicitly using the presented formulations (δ_{LE}), and the input signals are simply the factored combination of several signals via a finite difference scheme. The theoretical frameworks allowed for the application of BWIM algorithms to a broader set load effects. Two particular scenarios have been numerically investigated. The first study showed that multiple strain gauges BWIM systems might lead to consistently more accurate individual axle weight estimates, when compared to the standard one strain sensor BWIM. The second study explored an alternative way of establishing an acceleration-based BWIM. The results showed reasonably good average GVW estimates.

Declaration of Competing Interest

The authors declare that they have no known competing financial interests or personal relationships that could have appeared to influence the work reported in this paper.

Appendix A

See Table 3.

Table 3
Coefficients for the central finite difference schemes of order 1–4 with accuracy 2.

Order	Coeff.	Non-uniform grid	Uniform grid
1	$\alpha_{1,1}$	$\frac{x_2 - x_3}{(x_1 - x_2)(x - x_3)}$	$-\frac{1}{2h}$
	$\alpha_{1,2}$	$\frac{x_1 - 2x_2 + x_3}{(x_1 - x_2)(x_2 - x_3)}$	0
	$\alpha_{1,3}$	$-\frac{x_1 - x_2}{(x_1 - x_3)(x_2 - x_3)}$	$\frac{1}{2h}$
2	$\alpha_{2,1}$	$\frac{2}{(x_1 - x_2)(x_1 - x_3)}$	$\frac{1}{h^2}$
	$\alpha_{2,2}$	$-\frac{2}{(x_1 - x_2)(x_2 - x_3)}$	$-\frac{2}{h^2}$
	$\alpha_{2,2}$	$\frac{2}{(x_1 - x_3)(x_2 - x_3)}$	$\frac{1}{h^2}$
3	$\alpha_{3,1}$	$-\frac{6(x_2 - 3x_3 + x_4 + x_5)}{(x_1 - x_2)(x_1 - x_3)(x_1 - x_4)(x_1 - x_5)}$	$-\frac{1}{2h^3}$
	$\alpha_{3,2}$	$\frac{6(x_1 - 3x_3 + x_4 + x_5)}{(x_1 - x_2)(x_2 - x_3)(x_2 - x_4)(x_2 - x_5)}$	$\frac{1}{h^3}$
	$\alpha_{3,3}$	$-\frac{6(x_1 + x_2 - 4x_3 + x_4 + x_5)}{(x_1 - x_3)(x_2 - x_3)(x_3 - x_4)(x_3 - x_5)}$	0
	$\alpha_{3,4}$	$\frac{6(x_1 + x_2 - 3x_3 + x_5)}{(x_1 - x_4)(x_2 - x_4)(x_3 - x_4)(x_4 - x_5)}$	$-\frac{1}{h^3}$
	$\alpha_{3,5}$	$-\frac{6(x_1 + x_2 - 3x_3 + x_4)}{(x_1 - x_5)(x_2 - x_5)(x_3 - x_5)(x_4 - x_5)}$	$\frac{1}{2h^3}$
4	$\alpha_{4,1}$	$\frac{24}{(x_1 - x_2)(x_1 - x_3)(x_1 - x_4)(x_1 - x_5)}$	$\frac{1}{h^4}$
	$\alpha_{4,2}$	$-\frac{24}{(x_1 - x_2)(x_2 - x_3)(x_2 - x_4)(x_2 - x_5)}$	$-\frac{4}{h^4}$
	$\alpha_{4,3}$	$\frac{24}{(x_1 - x_3)(x_2 - x_3)(x_3 - x_4)(x_3 - x_5)}$	$\frac{6}{h^4}$
	$\alpha_{4,4}$	$-\frac{24}{(x_1 - x_4)(x_2 - x_4)(x_3 - x_4)(x_4 - x_5)}$	$-\frac{4}{h^4}$
	$\alpha_{4,5}$	$\frac{24}{(x_1 - x_5)(x_2 - x_5)(x_3 - x_5)(x_4 - x_5)}$	$\frac{1}{h^4}$

Appendix B

Eq. (22) and Eq. (23) show the Dirac delta function approximations obtained from rotations and deformations respectively. The formulation is based on the central finite difference scheme of accuracy 2. The formulation for a generic case with a non-uniform grid results in expressions that are too long to transcribe. Thus, the expressions below are for uniform grids, with a distance between points (or sensors) of h, and with the reference system located on the first point of the grid (i.e. $x_1 = 0$).

$$\delta_\theta(x_P) = \frac{1}{4\,\mathrm{EI}\,h^3}\begin{cases} 0 & x_P \le 0 \\ {x_P}^2 & 0 < x_P \le x_2 \\ 4\,h\,x_P - 2\,h^2 + {x_P}^2 & x_2 < x_P \le x_3 \\ 4\,h\,x_P - 2\,h^2 + {x_P}^2 & x_3 < x_P \le x_4 \\ (4\,h - x_P)^2 & x_4 < x_P \le x_5 \\ 0 & x_5 \le x_P \end{cases} \tag{22}$$

$$\delta_y(x_P) = \frac{1}{6\,\mathrm{EI}\,h^4}\begin{cases} 0 & x_P \le 0 \\ {x_P}^3 & 0 < x_P \le x_2 \\ 4\,h^3 - 12\,h^2\,x_P + 12\,h\,{x_P}^2 - 3\,{x_P}^3 & x_2 < x_P \le x_3 \\ -44\,h^3 + 60\,h^2\,x_P - 24\,d\,{x_P}^2 + 3\,{x_P}^3 & x_3 < x_P \le x_4 \\ (4\,h - x_P)^3 & x_4 < x_P \le x_5 \\ 0 & x_5 \le x_P \end{cases} \tag{23}$$

References

[1] Darren Hazlett, Nan Jiang, Lisa Loftus-Otway, Use of WIM data for pavement, bridge, weight enforcement, and freight logistics applications, Washington, DC: The National Academies Press; 2020. https://www.nap.edu/catalog/25793/use-of-weigh-in-motion-data-for-pavement-bridge-weight-enforcement-and-freight-logistics-applications.

[2] Technical Committee 4.3. Estimation of load carrying capacity of bridges based on damage and deficiency. World Road Association (PIARC); 2016. https://www.piarc.org/en/order-library/23963-en-Estimation%20of%20load%20carrying%20capacity%20of%20bridges%20based%20on%20damage%20and%20deficiency.htm.

[3] International Transport Forum (ITF). Polices to Extend the Life of Road Assets. ITF Research Reports, OECD Publishing, Paris, 2018. https://www.itf-oecd.org/policies-extend-life-road-assets.

[4] van Loo Hans, Žnidarič Aleš. Guide for users of weigh-in-motion. International Society for Weigh-in-Motion (ISWIM), Tiskarna knjigoveznica Radovljica, Ltd; 2019. http://www.is-wim.org/doc/ISWIM_Guide%20for%20users_press.pdf.
[5] Yu Yang, Cai CS, Deng Lu. State-of-the-art review on bridge weigh-in-motion technology. Adv Struct Eng 2016;19(9):1514–30. https://doi.org/10.1177/1369433216655922.
[6] Moses Fred. Weigh-in-motion system using instrumented bridges. ASCE Trans Eng J 1979;105:233–49.
[7] Lydon Myra, Taylor SE, Robinson D, Mufti A, OBrien EJ. Recent developments in bridge weigh in motion (B-WIM). J Civil Struct Health Monit 2016;6(1):69–81. https://doi.org/10.1007/s13349-015-0119-6.
[8] Cantero Daniel, Karoumi Raid, González Arturo. The Virtual Axle concept for detection of localised damage using Bridge Weigh-in-Motion data. Eng Struct 2015; 89:26–36. https://doi.org/10.1016/j.engstruct.2015.02.001.
[9] OBrien EJ, Quilligan MJ, Karoumi R. Calculating an influence line from direct measurements. Proc Instit Civ Eng - Bridge Eng 2006;159(1):31–4. https://doi.org/10.1680/bren.2006.159.1.31.
[10] Žnidarič Aleš, Kalin Jan. Using bridge weigh-in-motion systems to monitor single-span bridge influence lines. J Civil Struct Health Monit 2020;10(5):743–56. https://doi.org/10.1007/s13349-020-00407-2.
[11] Frøseth Gunnstein T, Rønnquist Anders, Cantero Daniel, Øiseth Ole. Influence line extraction by deconvolution in the frequency domain. Comput Struct 2017;189: 21–30. https://doi.org/10.1016/j.compstruc.2017.04.014.
[12] Zheng Xu, Yang Dong-Hui, Yi Ting-Hua, Li Hong-Nan, Chen Zhi-Wei. Bridge influence line identification based on regularized least-squares QR decomposition method. 06019004 J Bridge Eng 2019;24(8). https://doi.org/10.1061/(ASCE)BE.1943-5592.0001458.
[13] Chen Zhiwei, Yang Weibiao, Li Jun, Yi Tinghua, Wu Junchao, Wang Dongdong. Bridge influence line identification based on adaptive B-spline basis dictionary and sparse regularization. Struct Control Health Monit 2019; 26: e2355. DOI: 10.1002/stc.2355.
[14] Zheng Xu, Yang Dong-Hui, Yi Ting-Hua, Li Hong-Nan. Bridge influence line identification from structural dynamic responses induced by a high-speed vehicle. Struct Control Health Monit 2020; 27: e2544. DOI: 10.1002/stc.2544.
[15] Yan Wang-Ji, Yuen Ka-Veng. A new probabilistic frequency-domain approach for influence line extraction from static transmissibility measurements under unknown moving loads. Eng Struct 2020; 216: 110625. DOI: 10.1016/j.engstruct.2020.110625.
[16] He Wei, Deng Lu, Shi Hai, Cai CS, Yu Yang. Novel virtual simply supported beam method for detecting the speed and axles of moving vehicles on bridges. ASCE J Bridge Eng 2017; 22(4): 04016141. DOI: 10.1061/(ASCE)BE.1943-5592.0001019.
[17] Chen Shi-Zhi, Wu Gang, Feng De-Cheng, Zhang Lu. Development of a bridge weigh-in-motion system based on long-gauge fiber bragg grating sensors. ASCE J Bridge Eng 2018; 23(9): 04018063. DOI: 10.1061/(ASCE)BE.1943-5592.0001283.
[18] Chen Shi-Zhi, Wu Gang, Feng De-Cheng. Development of a bridge weigh-in-motion method considering the presence of multiple vehicles. Eng Struct 2019;191: 724–39. https://doi.org/10.1016/j.engstruct.2019.04.095.
[19] Fornberg Bengt. Calculation of weights in finite difference formulas. Soc Ind Appl Math, SIAM REV 1998;40(3):685–91.
[20] Chen Shi-Zhi, Wu Gang, Feng De-Cheng. Damage detection of highway bridges based on long-gauge strain response under stochastic traffic flow. Mech Syst Sig Process 2019;127:551–72. https://doi.org/10.1016/j.ymssp.2019.03.022.
[21] Cantero Daniel, Obrien Eugene J, González Arturo. Modelling the vehicle in vehicle–infrastructure dynamic interaction studies. Proc Instit Mech Eng. Part K – J Multi-body Dynam 2009; 224(2): 243–248. DOI: 10.1243/14644193JMBD228.
[22] González Arturo, Cantero Daniel, Obrien Eugene J. Dynamic increment for shear force due to heavy vehicles crossing a highway bridge. Comput Struct 2011; 89: 2261–2272. DOI: 10.1016/j.compstruc.2011.08.009.
[23] International Organization for Standardization. Mechanical vibration – road surface profiles – reporting of measure data. ISO 8608; 1995.
[24] McLean DI, Marsh ML. Dynamic impact factors for bridges. NCHRP Report 266, Transportation Research Board, Washington D.C.; 1998.
[25] Žnidarič Aleš, Turk G, Zupan E. Determination of strain correction factors for bridge weigh-in-motion systems. Eng Struct 2015;102:387–94. https://doi.org/10.1016/j.engstruct.2015.08.026.
[26] Sekiya Hidehiko, Kubota Kosaku, Miki Chitoshi. Simplified portable BWIM system using accelerometers. ASCE. 04017124 J Bridge Eng 2018;23(1). https://doi.org/10.1061/(ASCE)BE.1943-5592.0001174.
[27] Sekiya Hidehiko. Field verification over one year of a portable bridge weigh-in-motion system for steel bridges. ASCE J Bridge Eng 2019; 24(7): 04019063. DOI: 10.1061/(ASCE)BE.1943-5592.0001411.
[28] Obrien Eugene, Khan Muhammad Arslan, McCrum Daniel, Žnidarič Aleš. Using statistical analysis of an acceleration-based BWIM for damage detection. MDPI Appl Sci 2020; 10: 663. DOI: 10.3390/app10020663.